Title: How to Model Cooling Service Flow of Urban Parks Based on Supply-Flow-Demand Framework? A Case Study of Beijing Olympic Park

Authors:

Yufan Wang (yufanwangbjfu@foxmail.com), Beijing Forestry University School of Ecology and Nature Conservation, No. 35 East Qinghua Road, Haidian District, Beijing 100083(zip code) P. R. China.

Fengchen Li (lifengchen@bjfu.edu.cn), Beijing Forestry University School of Ecology and Nature Conservation, No. 35 East Qinghua Road, Haidian District, Beijing 100083(zip code) P. R. China.

Jiyao Li (2485067743@qq.com), Beijing Forestry University School of Ecology and Nature Conservation, No. 35 East Qinghua Road, Haidian District, Beijing 100083(zip code) P. R. China.

Zeyu He (hzey163@163.com), Beijing Forestry University School of Ecology and Nature Conservation, No. 35 East Qinghua Road, Haidian District, Beijing 100083(zip code) P. R. China.

Yunhan Dong (3234744981@qq.com), Beijing Forestry University School of Ecology and Nature Conservation, No. 35 East Qinghua Road, Haidian District, Beijing 100083(zip code) P. R. China.

Jie Xu (Corresponding Author) (jiexu@bjfu.edu.cn) (+86 15010669728), Beijing Forestry University School of Ecology and Nature Conservation, No. 35 East Qinghua Road, Haidian District, Beijing 100083(zip code) P. R. China.

Coversheet Statement:

This manuscript is a non-peer reviewed preprint submitted to EarthArXiv.

It has also been submitted for peer review to Sustainable Cities and Society on 2025/5/16.

Abstract:

Rapid urbanization intensifies the urban heat island effect and undermines health for vulnerable communities located beyond the effective cooling reach of large parks. This study introduced a spatially supply-flow-demand framework to quantify the cooling service flow of urban park using Beijing Olympic Park as a case study. Field measurements at representative land types in the park were integrated with local parameter as inputs to model supply. To link supply with demand, we designed a grid system with cells of approximately 500 m covering 8 km*10 km area around the park, set a scenario of removing the park and compared it with the existing scenario to simulate the effect of park, so that we can qualify building-level demand. The analysis produced preliminary maps of cooling flow of Beijing Olympic Park. Results revealed that inside the park the cooling supply varied significantly by land types and seasons. Outside the park service flow of the park attenuated rapidly beyond 1 km and 1-2 km buffer zone from the park edge exhibited unmet needs of up to 7.5℃. To integrate supply and demand into a more comprehensive evaluation map, we built adjustment gap priority map and found that the southern buffer area of the park which is closer to the city center has the most urgent demand relatively. In summary, this transferable framework offers urban planners a data-driven tool for more equitable and effective green infrastructure investment.

Keywords: Ecosystem Service Flow, Urban Park, Urban Heat Island Mitigation, Spatial Mismatch Analysis.

1. Introduction

Cities are central to global climate change mitigation, serving as home to over half of the world's population and accounting for approximately 75% of global energy consumption and greenhouse gas emissions (Mi et al., 2019; Xiong et al., 2019). However, in the face of increasingly extreme summer temperatures, dense built environments and impervious surfaces have intensified urban heat island (UHI) effects, contributing to higher rates of mortality, morbidity, and psychological distress (Ebi et al., 2021; Markevych et al., 2017; Mashhoodi, 2021). The growing reliance on air conditioning to maintain indoor thermal comfort further compounds the problem, as waste heat from cooling systems exacerbates ambient urban temperatures (Jay et al., 2021). In contrast to these unsustainable cooling strategies, large urban parks as key components of green infrastructure offer a nature-based alternative (Li et al., 2021; Lin et al., 2021). Through the combined effects of vegetation, water bodies, and heterogeneous landscape patches, such parks can lower surrounding temperatures by 4 to 4.5 °C and significantly reduce building energy demand (Aflaki et al., 2017). The extent and intensity of this cooling effect depend on factors such as park size, patch composition and quality, and the permeability and structure of adjacent urban morphology (Aram et al., 2019). Yet, it remains unclear how far these cooling services extend beyond park boundaries and whether they effectively reach areas with the highest cooling needs. The knowledge gap limits the ability of planners and policymakers to harness urban parks for equitable and efficient climate adaptation (Xiao et al., 2023).

The cooling capacity of urban parks, as a key ecosystem service, has been extensively examined through the lens of supply sources, flow processes, and human demand (Aram et al., 2019). One group of research compares the cooling performance of multiple parks using various indicators, linking observed differences to landscape configuration (Lai et al., 2024; Lan et al., 2025; Yang et al., 2024). Zeng et al. (2024) used a three-step Huff model to evaluate population attractiveness based on trip distance and cooling potential; Wang et al. (2024) developed spatial indices for both cooling supply and demand to reveal mismatches, and Liyan et al. (2023) integrated thermal exposure with population sensitivity, highlighting high stress in vulnerable communities and unequal vegetation resource allocation. Most of these studies rely heavily on remote sensing data, such as land surface temperature retrieval and NDVI, while only a limited number incorporate field-based meteorological data to validate model outputs (Amani-Beni et al., 2018; Gao et al., 2023; Wolff et al., 2015). A second group of studies adopts scenario-based simulations to evaluate the thermal performance of green space–building configurations, with ENVI-met being the most commonly used tool (Alves et al., 2022; Mosteiro-Romero et al., 2020) . However, its computational limits restrict simulations to neighborhood scales within roughly 1 km². More recently, computational fluid dynamics approaches have emerged, integrating satellite imagery, in-situ measurements, and thermal imaging for validation (Buccolieri et al., 2018; Toparlar et al., 2017; Yang et al., 2023) . Despite these advances, demand-side considerations remain underexplored and most studies lack quantitative assessment of how much cooling is actually needed in the service-receiving areas (Fang et al., 2024) . Existing demand analyses are often limited to qualitative evaluations or single supply-demand balance indices (Fang and Zhao, 2024; Li and Sun, 2023a) . Some recent efforts have employed quadrant-based frameworks to characterize the spatial alignment or mismatch between supply and demand, but few have successfully integrated supply, flow, and demand within a unified spatial framework (R. Wang et al., 2024; Y. Wang et al., 2024).

To address the gaps identified above, this study proposes a unified framework for quantifying cooling service flows across continuous urban space using a consistent spatial unit. Focusing on Beijing Olympic Park as a case study, we integrated field-measured meteorological data with the Urban Cooling Model from the Integrated Valuation of Ecosystem Services and Tradeoffs (InVEST) toolset. This approach enabled us to assess not only the spatiotemporal heterogeneity of cooling intensity across different land cover types within the park, but also the park's overall role as a cooling service source and its diffusion into surrounding urban areas. Crucially, we linked modeled cooling supply with building-level thermal demand, incorporating height-based energy sensitivity to reflect variation in air-conditioning needs. This coupling revealed spatial mismatches between supply and demand that conventional greening metrics fail to capture. By introducing a gridded spatial indicator Cooling Priority Score, we identified urban hotspots with the greatest need for heat mitigation. This approach shifts the focus from the mere presence of green space to its functional performance in heterogeneous urban environments, offering a transferable method for diagnosing and addressing urban heat risks through more targeted and spatially equitable green infrastructure planning.

2. Methods

2.1. Study Area

Beijing, in a warm temperate semi-humid monsoon zone, has hot, humid summers and cold, dry winters. Rapid urbanization has intensified the urban heat island effect, reducing comfort and increasing energy use. Covering roughly 680 hectares, Beijing Olympic Park is the city's largest urban green space and comprises northern and southern sections connected by a central corridor. Its mixed land cover including arbor forest, grassland, shrubland, water, and wetland provides key ecological buffering (Amani-Beni et al., 2018) . A 2,000 m buffer around Beijing Olympic Park (Figure 1b), based on literature estimates of urban park cooling reach, defines the study area (N. Zhang et al., 2024). To evaluate Beijing Olympic Park's cooling effect of different land type inside, 19 fixed meteorological stations were selected (Figure 1c). Station IDs combining a number and land cover label reflect iterative validation across four sampling months, with only stable representative points retained, therefore not continuous (Table 1).

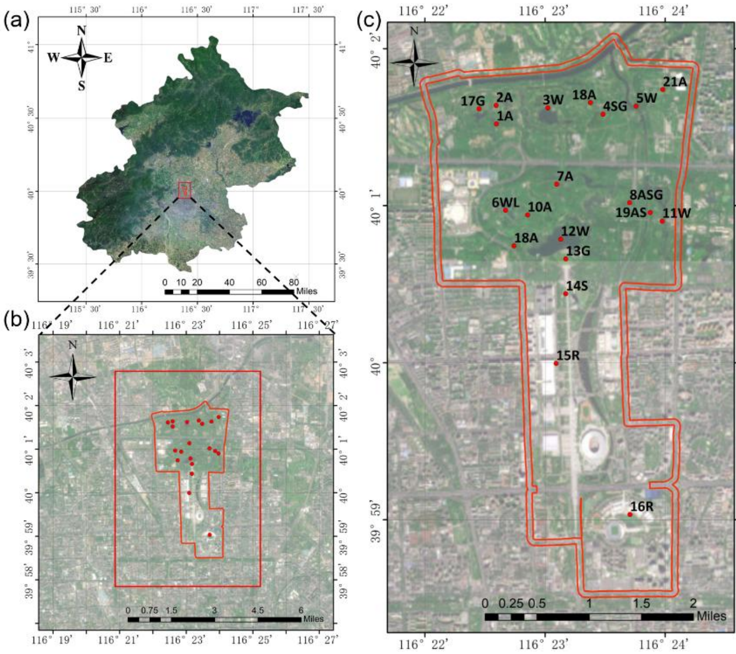

(d)

point location	vegetation type	Abbreviation
1	arbor	A
2	arbor	A
3	water	W
4	shrub&grass	SG
5	water	W
6	wetland	WL
7	arbor	A
8	arbor&shrub &grass	ASG
10	arbor	A
11	water	W
12	water	W
13	grass	G
14	shrub	S
15	road	R
16	road	R
17	grass	G
18	arbor	A
19	arbor&grass	AG
21	arbor	A

Figure 1. Study area and monitoring layout. (a) Location of Beijing Olympic Park, China. (b) 2,000 m buffer zone representing the maximum green space cooling extent. (c) Fixed monitoring sites across representative land cover types. (d) Land cover types corresponding to sample sites.

2.2. Field Monitoring Design

To evaluate Beijing Olympic Park's cooling performance during peak thermal periods, field measurements were conducted in August and September 2023, and June and August 2024. Observations were made between 9:00–18:00 on clear, calm, rain-free days using Kestrel NK5500 Weather Meter at 1.5 m height. All data were collected by the same team members along a fixed route to ensure consistency, the fixed points were deployed across major land cover types, as listed in Figure 1 (d).

To capture thermal gradients around the park, two concentric transects were set up: the inner loop along the park-facing road and the outer loop on the opposite side, representing urban background. Walk-throughs in the morning (9:00-10:00), noon (12:00-13:00), and afternoon (17:00-18:00) recorded temperature, humidity, and wind every minute, enabling continuous microclimate profiling across distances from the park edge.

2.3. Data Analysis

2.3.1. Quantifying Park Inner Cooling Service Supply Difference

To assess localized cooling service from green and blue infrastructure, we first analyzed midday fluctuations in Heat Index (HI), which combined air temperature and relative humidity to reflect perceived thermal stress. For comparability, we used average HI values from 12:00 to 15:00 to represent peak thermal exposure, which were visualized using boxplots. To further examine how temperature varied over the course of the day, we conducted paired-point comparisons between selected vegetated or aquatic sites and nearby bare-surface controls (<10 m apart).

2.3.2. Modeling Spatial Flow of Cooling Services

Point-based monitoring reveals localized cooling effect but cannot capture the full 2 km spatial extent of park's thermal regulation. To overcome this, we used the InVEST Urban Cooling Model to simulate heat mitigation based on land cover and biophysical properties (Table 1). Two land use scenarios, derived from 2023-2024 satellite imagery, were compared: a bare land scenario, where the park was replaced with barren land to represent pre-development conditions, and a green infrastructure scenario, which retained actual green and blue area. Surrounding urban areas were held constant, and other green spaces within the area were excluded, allowing for isolation of the park's cooling contribution (Figure 2).

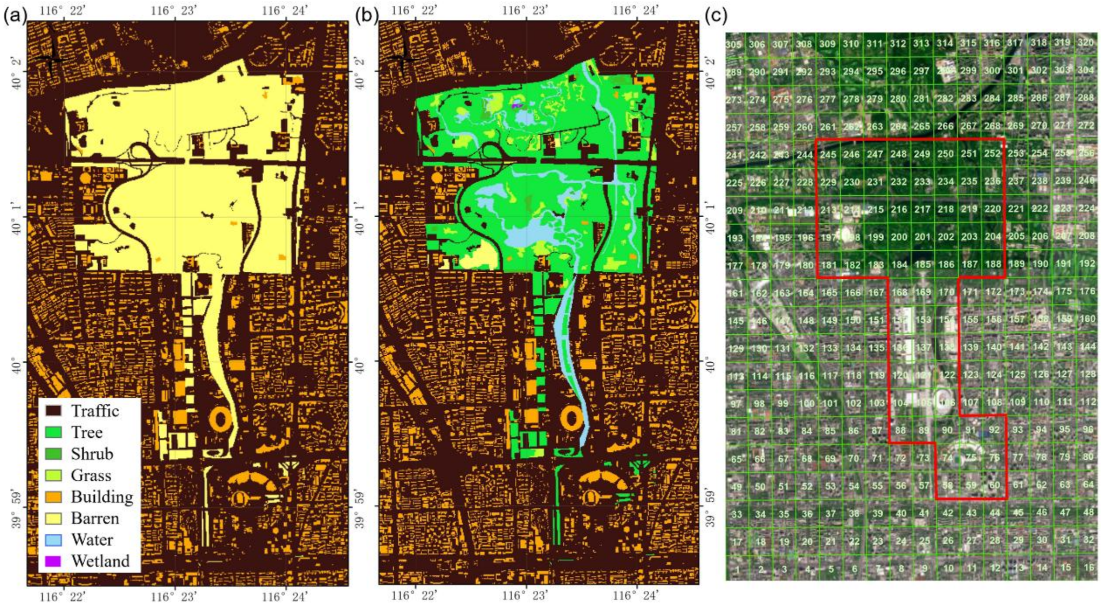

Figure 2. Land cover classifications under two simulation scenarios for the InVEST Urban Cooling Model. (a) Bare land scenario: the entire Beijing Olympic Park is replaced with barren land.(b) Green infrastructure scenario: actual land cover types within the park. (c) Grid-based spatial area for InVEST analysis, the red frame represents the park boundary.

Model Configuration and Input Data

The model was parameterized with local environmental data and field observations. Key inputs included a reclassified land use raster, ET_0 was calculated via the FAO Penman-Monteith method, and a biophysical table detailing Kc, albedo, shade fraction, and building intensity by land cover. The area of interest was a 2,000 m buffer around Beijing Olympic Park, reflecting the typical cooling reach of urban parks. The maximum urban heat island magnitude was based on the observed urban–rural temperature difference on the hottest day, and reference air temperature was set to the rural daytime average. Heat dispersion was modeled with a 200 m air blending distance and a 2,000 m maximum cooling distance. Biophysical parameters were locally adapted from existing InVEST studies (Table 1).

lucode	Kc	green_area	shade	albedo	building_intensity	Land Use/Land Cover
2	1	1	0.8	0.15	0	tree
3	0.8	1	0.1	0.2	0	shrub

4	0.6	1	0	0.2	0	grass
6	0	0	0	0.2	0.9	building
1	0	0	0	0.1	0	traffic
7	0.2	0	0	0.25	0	barren
9	1.2	1	0	0.08	0	water
10	1	1	0.1	0.15	0	wetland

Table 1. Corresponding parameter Settings for various land cover types

For energy savings estimation, buildings were grouped into five height classes (3.5–100 m), each assigned a cooling energy coefficient: 0.10 (Type 1: 3.5–10 m), 0.15 (Type 2: 10–18 m), 0.22 (Type 3: 18–24 m), 0.35 (Type 4: 24–54 m), and 0.55 (Type 5: 54–100 m). Relative humidity was included for productivity valuation. Cooling capacity weights followed established defaults: 0.6 for shade, 0.2 for albedo, and 0.2 for evapotranspiration.

Cooling Index Calculation and Heat Diffusion Simulation

The InVEST Urban Cooling Model estimates grid-level cooling capacity (CC) based on land surface characteristics. CC is computed as a weighted combination of three variables: vegetation shade (canopy cover > 2 m^2), surface albedo, and evapotranspiration potential. The evapotranspiration index ETI is calculated as:

$$ETI_i = \frac{K_c(i) \cdot ET_0(i)}{ET_{max}}$$

where K_c is the crop coefficient for each land cover type (shown in Table 1), ET_0 is the reference evapotranspiration, and ET_{max} is the maximum across the landscape. To localize ET_0 values, we applied the empirical equation by Droogers & Allen (2002) using field temperature data from August and September 2023, and June and August 2024:

$$ET_0 = 0.0023 \cdot 0.408 RA\left(T_{avg} + 17.8\right) \cdot TD^{0.5}$$

where RA is extraterrestrial radiation, T_{avg} is daily mean temperature, and TD is diurnal temperature range. The three components are integrated into a composite index:

$$CC_i = 0.2 \cdot shade_i + 0.2 \cdot albedo_i + 0.6 \cdot ETI_i$$

To simulate spatial heat mitigation, the Heat Mitigation Index (HMI) is calculated. For pixels near green infrastructure (>2 ha), HMI_i is a distance-weighted average of surrounding green-space CC_i values; otherwise, HMI_i equals the local CC:

$$HMI_i = \begin{cases} CC_i, \ \ if\ CC_i \geq CC_{park}\ or\ GA_i < 2ha \\ CC_{park}, \ \ otherwise \end{cases}$$

The pixel-level air temperature without air mixing $T_{air,nomix,\ i}$ is then estimated as:

$$T_{air,nomix,\ i} = T_{air,ref} + (1 - HM_i)\cdot UHI_{max}$$

This intermediate result is spatially smoothed using a Gaussian kernel function over the blending distance r, producing the final modeled air temperature surface $T_{air,\ i}$. The temperature anomaly is subsequently calculated as:

$$T_{anomaly} = T_{air,i} - T_{air,ref}$$

If enabled, the model also estimates energy savings per building polygon as:

$$Energy.saving_b = comsumption.increase(b)\cdot(\overline{T_{air,max} - T_{air,i}})$$

where $T_{air,max}$ is the maximum temperature in the area of interest and $T_{air,i}$ is the local air temperature.

Model Outputs

The InVEST Urban Cooling Model produces spatial outputs that quantify urban cooling. Central among these is the HMI, which reflects grid-level cooling based on land cover and green infrastructure proximity. The model also generates urban temperature surfaces, allowing for the identification of temperature anomalies relative to rural baselines. When valuation modules are enabled, it estimates building-level energy savings and productivity gains using temperature reductions. These outputs aid in assessing cccoling service flows and spatial mismatches between thermal regulation supply and demand.

Spatial Gridding and Temperature Difference Mapping

To evaluate the spatial distribution of cooling services, we overlaid a 16*20 uniform grid (total 320 cells) across the 2,000 m buffer surrounding Beijing Olympic Park. Each grid cell served as a consistent unit for temperature aggregation and comparison, balancing spatial resolution with computational efficiency for urban-scale analysis.

Analyses focused on building land type (lucode = 6) to reflect human related thermal exposure. For each grid cell, average temperatures were calculated under both vegetated (veg) and barren (bare) scenarios, and the cooling effect was derived as:

$$\Delta T = T_{bare} - T_{veg}$$

Where T_{bare} and T_{veg} denote the average building temperature in each grid cell under the corresponding scenario. Grid cells without valid building data were retained as NaN. The results were visualized as gridded maps, indicating spatial variability in temperature mitigation.

2.3.3. Identifying Cooling Demand and Gaps

To evaluate cooling service adequacy, we employed the same 16*20 grid to quantify supply, demand, and regulation gaps using valid building pixels. Cooling demand represented the exceedance of the comfort threshold (set as 26 °C, a commonly adopted benchmark for summer outdoor comfort in northern China) under the vegetated scenario, while supply was the temperature reduction from barren scenario to vegetated scenario. Their difference indicated unmet cooling needs.

Cooling demand per grid cell was calculated as the degree to which average air temperature under the vegetated scenario exceeded 26°C and the calculation was formalized as:

$$Cooling\ Demand_i = max(0, T_{veg,i} - 26)$$

where $T_{veg,i}$ is the mean temperature of building pixels within grid cell i in the vegetated scenario. Values were set as 0 for cells where average temperatures fell below the comfort threshold.

Cooling supply was calculated for each grid cell as the temperature reduction attributable to green infrastructure, represented by the temperature difference between the barren scenario and vegetated scenario:

$$Cooling\ Supply_i = T_{bare,i} - T_{veg,i}$$

where both values were computed as the average temperature across all building pixels within grid cell i under each respective scenario.

The cooling gap was computed as the difference between demand and supply, reflecting the magnitude of unmet cooling needs:

$$Cooling\ Gap_i = Cooling\ Demand_i - Cooling\ Supply_i$$

All three metrics were calculated consistently across all grid cells for each monitoring period. For broader spatial analysis, grid cells were aggregated into three concentric zones based on distance from the park boundary, facilitating comparative assessment of spatial patterns as park area, 0–1 km buffer and 1-2km buffer.

Cooling Priority Score Estimation

To identify areas most in need of thermal mitigation, we developed a cooling priority score (CPS) that integrated ambient temperature and energy sensitivity and the score was also calculated for each cell in the 16*20 grid using:

$$CPS_i = (T_{bare,i} - 26) \cdot CF_i$$

where $T_{bare,i}$ is the modeled temperature in cell i under the barren scenario, and 26 °C is the thermal comfort threshold. CF_i represents the energy consumption coefficient based on building height, with taller structures assigned higher values due to greater cooling demand. CPS_i was computed for building pixels (lucode = 6) with valid height classifications and then averaged within each grid cell.

3. Results

3.1. Variation in Local Cooling Supply by Land Cover Type

Monitoring results showed daily HI variations, reinforcing that tree covered sites (Points 2, 7, 13) consistently offered the strongest and most stable cooling. Water sites (Points 3, 5, 11) had low but variable HI values, influenced by external conditions. Grass and shrub sites (Points 4, 8, 17) provided moderate, less stable cooling, while impervious surfaces (Points 10, 16) showed consistently high and variable HI, indicating limited thermal regulation capacity.

Spatially, Beijing Olympic Park’s cooling services varied significantly by land cover. Tree sites delivered sustained, robust cooling via combined shading and evapotranspiration, maintaining lower daytime peaks and smoother temperature profiles. Water sites provided intermittent evaporative cooling, sensitive to meteorological fluctuations. Grass and shrub sites offered limited cooling due to the absence of shade, quickly reaching cooling limits under intense sunlight. Thus, trees emerged as the most reliable cooling provider, whereas other surfaces offered diminishing or variable benefits.

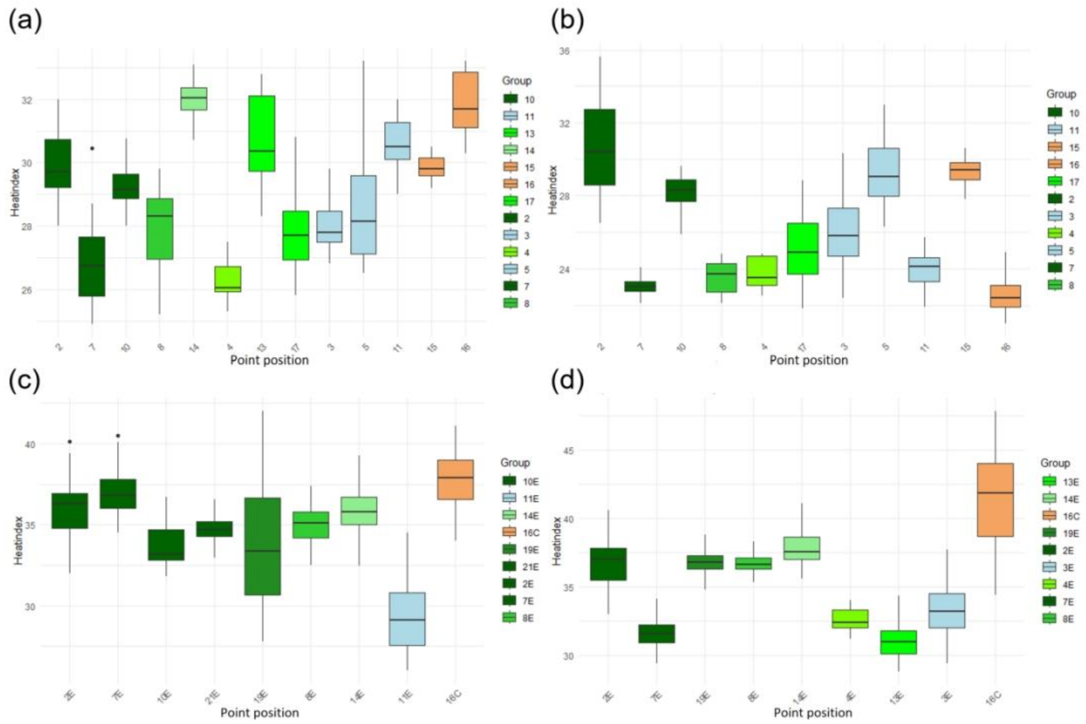

Figure 3. HI variability across land cover types and monitoring periods. (a) August 2023; (b) September 2023; (c) June 2024; (d) August 2024.

The diurnal HI curves further illustrate these differences under peak summer conditions. Across all sites, impervious control points showed sharp, early-afternoon HI peaks often surpassing 40 °C, reflecting intense heat buildup. In contrast, vegetated or water experimental sites demonstrated flattened HI curves with delayed, lower peaks, highlighting their thermal buffering capacity. Among them, tree-covered sites exhibited both lower maxima and smoother curves, due to consistent shading and evapotranspiration. Water sites showed moderate but variable cooling effects, while mixed sites exhibited modest thermal moderation, though with some afternoon flattening that suggested a degree of cumulative moisture driven cooling. These temporal profiles reinforced the previously observed cooling hierarchy, arbor > water ≈ grass/shrub > impervious.

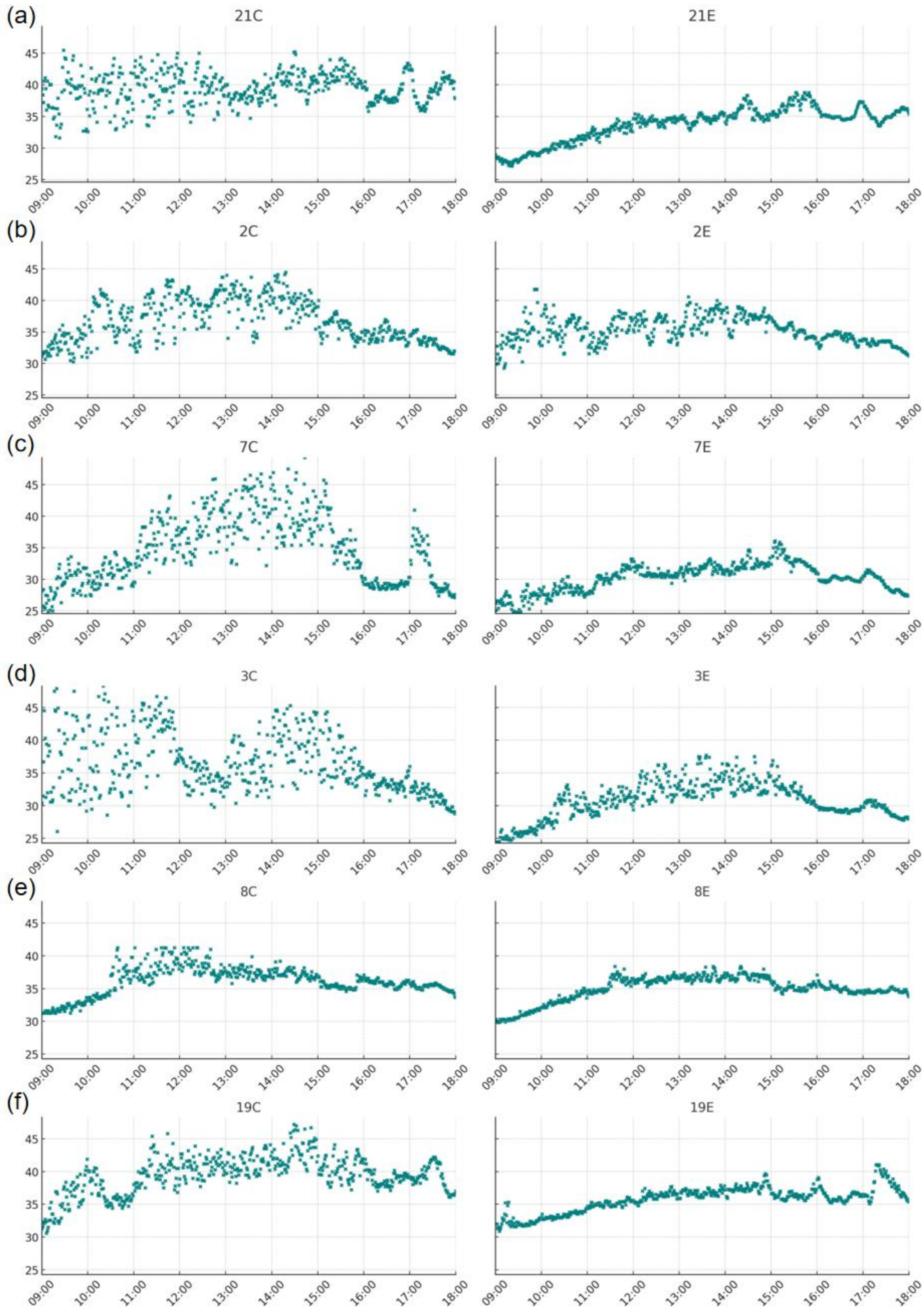

Figure 4. Diurnal variation trend of green or blue land HI compared with the control group placed in the surrounding barren land. C represents the control group and E represents the experimental group. (a) Tree Point 21; (b) Tree Point 2; (c) Tree Point 7; (d) Water Point 3; (e) Arbor&shrub&grass Point 8; (f) Arbor&shrub&grass Point 19.

3.2. Spatial Diffussion of Park Cooling Service Flow

The InVEST modeled cooling service flow revealed a distinct spatial gradient centered on Beijing Olympic Park. As shown in Figure 5(a), HMI values peaked within the park (~0.78) and declined radially, forming concentric isolines that extended up to ~2 km—a pattern consistent with empirical studies of urban park cooling footprints. This radial attenuation confirmed the model's ability to capture long-range cooling beyond field observation limits. Figures 5 (b) - (d) zoomed into buffer sectors, illustrating that areas adjacent to the park with substantial vegetation maintained moderate HMI values (0.2–0.3), while distant or impervious zones dropped below 0.1, highlighting the key role of proximity and land cover continuity in receiving cooling benefits. The cooling effect was detectable up to 1.5-2 km from the park center under peak summer conditions, though it diminished rapidly beyond ~1 km. As cool air moves outward, it mixes with ambient urban air, reducing the temperature gradient. Thus, residents within ~1 km of the park can expect meaningful cooling, while those beyond receive minimal benefit.

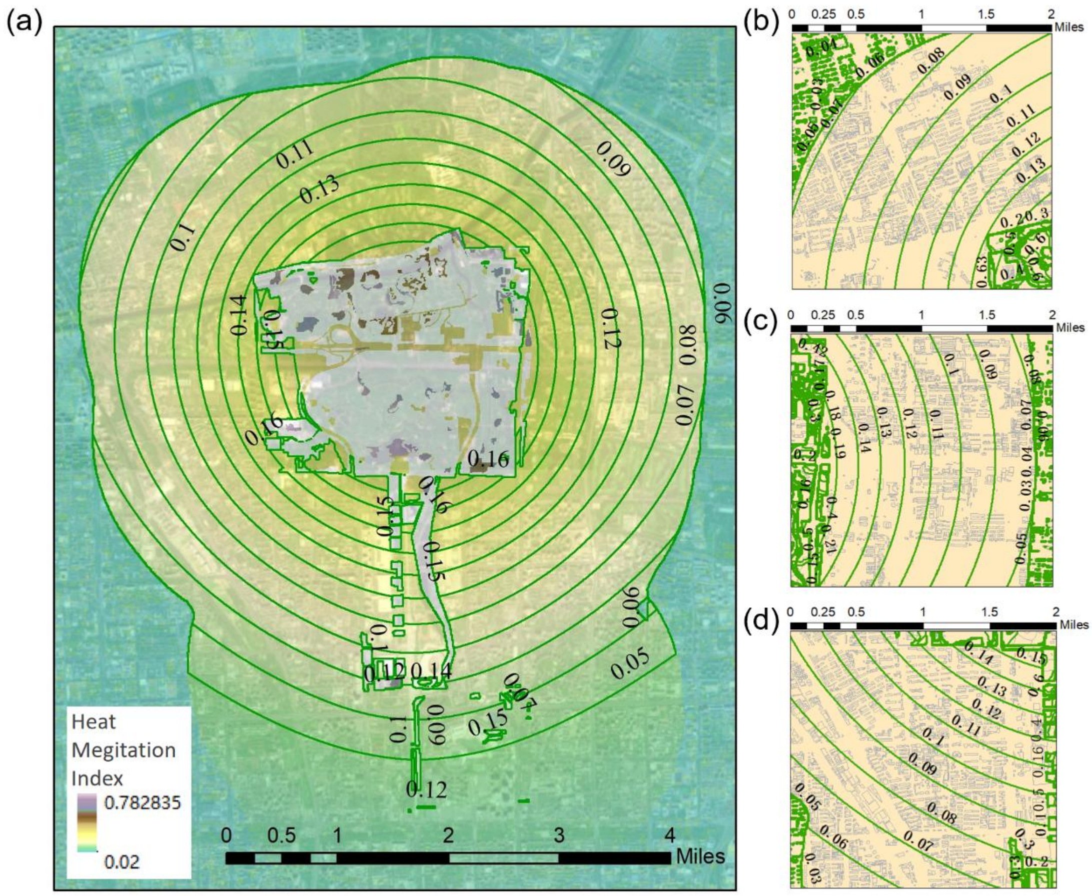

Figure 5. Spatial distribution of Heat Mitigation Index (HMI) modeled by the InVEST Urban Cooling Model. (a) Overall cooling flow pattern radiating from the park core. (b) Localized HMI distribution in the northwest corner of park. (c) Localized HMI distribution in the eastern section of the park. (d) Localized HMI distribution in the southwest corner of the park.

Building on this spatial trend, Figure 6 showed modeled temperature differences between vegetated and barren scenarios across four months. The park core exhibited the strongest effect (~2.5 °C), particularly in August, aligning with peak thermal stress. Outer zones saw limited mitigation (<0.5 °C), emphasizing the park's restricted reach into the broader urban matrix. Importantly, the spatial configuration of the surrounding urban form shaped the extent of cooling diffusion. Green corridors and low-rise open layouts facilitated deeper cooling penetration in the northeast and on both sides of the park. In contrast, high-density, impervious developments on the park's south side created thermal barriers. This is consistent with findings by Upmanis et al. (1998), Norton et al. (2015), and Sugawara et al. (2021), who noted that vegetated or ventilated urban fabrics enhance the spillover cooling effect of parks.

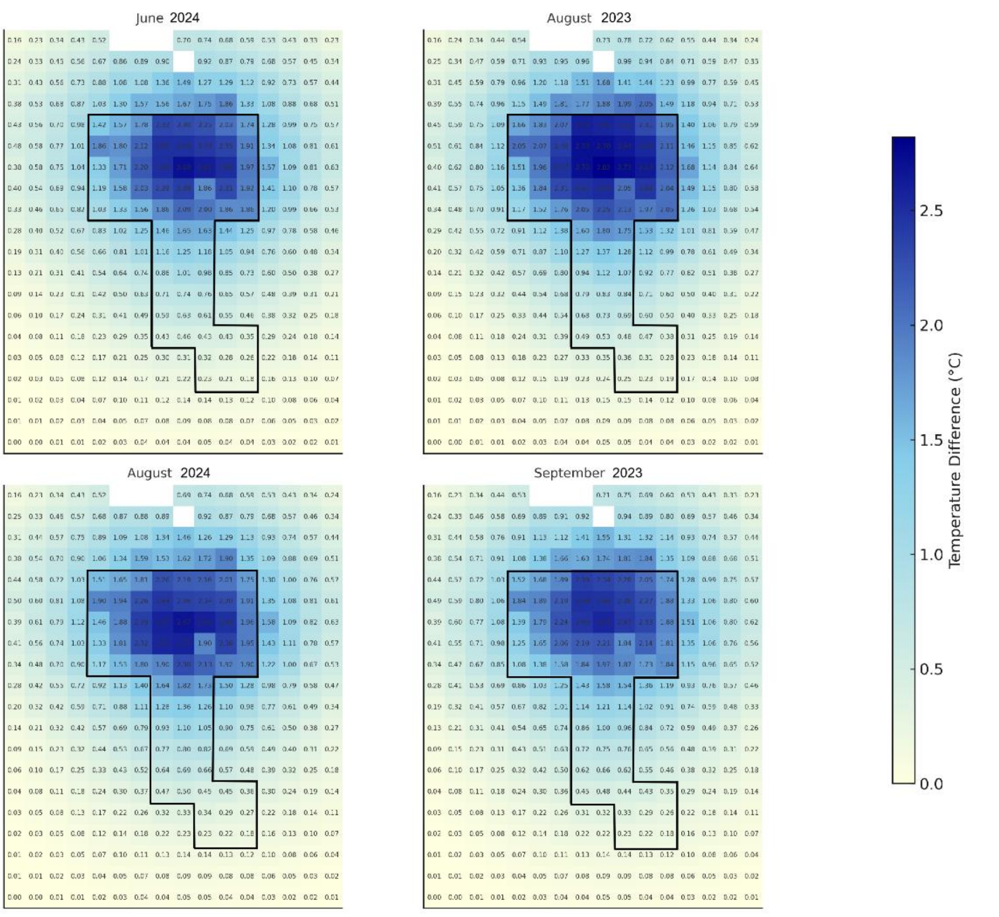

Figure 6. Spatial distribution pattern of temperature reduction across four month (June 2024, August 2023, August 2024, September 2023), the black frame represents the park boundary, and the blank grid means that there are not enough buildings in this block for modeling.

3.3. Spatial Mismatch Between Cooling Demand and Supply

Cooling demand exhibited a clear spatial gradient, increasing with distance from the green core. In the park area, thermal demand remained consistently low (7.31 ℃), while it rised slightly in the 0–1 km zone (7.32 ℃) and peaked in the 1–2 km zone at 7.79 ℃ across all months. This reflected the combined effects of reduced vegetation cover and intensified urban heat exposure, although Beijing Olympic Park effectively cools its immediate surroundings, more distant zones that are typically residential and densely urbanized tend to accumulate substantial thermal stress.

In contrast, the strongest cooling supply was observed within the park itself, reaching up to 2.05 ℃ in August 2023, and decreased significantly beyond its boundary. In the 0-1 km zone, cooling supply remained moderate, ranging from approximately 1.83 to 2.03 ℃. However, in the 1 to 2 km zone, the supply declined sharply and did not exceed 0.24 ℃. This spatial mismatch led to a significant regulation gap, with unmet cooling needs reaching up to around 7.56 ℃ in the 1 to 2 km ring. These peripheral neighborhoods were located mostly to the south and west, and often coincided with zones of dense built infrastructure, including high-rise residential and commercial districts with limited vegetation, which intensified local heat while receiving minimal cooling benefits from the park.

Table 2. Cooling demand, supply, and gap across park core and surrounding buffer zones.

month	zone	cooling_demand	cooling_supply	cooling_gap
August 2023	Park Area	7.31	2.05	5.26
	0–1 km Buffer	7.32	2.03	5.28
	1–2 km Buffer	7.79	0.24	7.55
September 2023	Park Area	7.31	1.84	5.47
	0–1 km Buffer	7.32	1.83	5.49
	1–2 km Buffer	7.79	0.23	7.56
June 2024	Park Area	7.31	1.86	5.46
	0–1 km Buffer	7.32	1.84	5.48
	1–2 km Buffer	7.79	0.23	7.56
August 2024	Park Area	7.31	1.90	5.41
	0–1 km Buffer	7.32	1.89	5.43
	1–2 km Buffer	7.79	0.23	7.56

A clear spatial mismatch emerged between the modeled cooling demand and the actual supply. Peak thermal stress rose above 7.6℃ across the park core and its surrounding areas in the demand modeling result, underscoring the intense urban heat buildup that lacked vegetative relief. Yet the park's cooling effect did not align with this demand. In the supply result, the park achieved a notable cooling supply exceeding 2.5℃ at its center, but this benefit diminished rapidly with distance. Consequently, the regions experiencing the greatest thermal demand roughly 1-2 km from the park's edge received the smallest cooling benefit. Our results indicate that beyond 1 km the supply typically fell below 0.3℃ while local demand could climb to approximately 7.5℃.

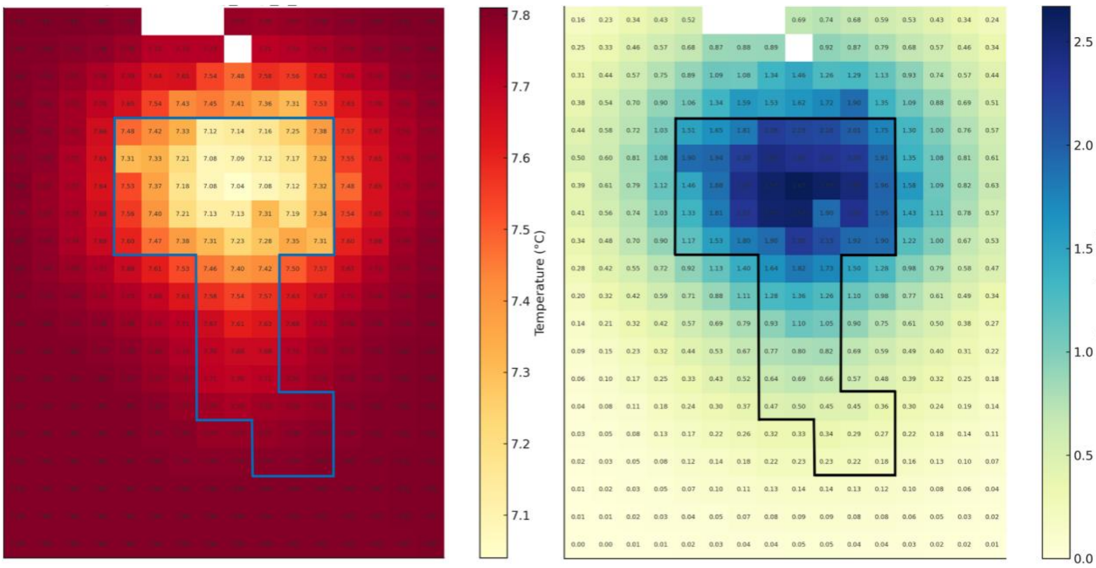

Figure 7. Spatial distribution pattern of service supply and demand pairing. Left: Cooling Demand of urban space without green space; Right: Cooling supply in the scenario with green space.

The spatial pattern of adjustment gap priority results from combining thermal stress intensity with the potential energy burden caused by insufficient cooling. Cells in the park's extensive contiguous green areas exhibited the lowest gap scores and often remained below 0.8 °C because high cooling supply around 2.0 °C balanced moderate demand near 7.3 °C, demonstrating an effective service. In the zone 0-1 km beyond the park edge, patterns were more varied. Some cells located along vegetated corridors still received residual regulation, yet many areas adjacent to arterial roads or surrounded by impervious surfaces showed gap scores above 1.2 to 1.5 °C. These values reveal a partial shortfall in cooling service where the urban layout hindered heat mitigation despite the short distance to the park. The most pronounced gaps occurred in the 1-2 km buffer beyond the park, particularly in the southeastern fringe, where gap scores rose above 1.8 °C. In those neighborhoods demand peaked at nearly 7.5 °C while cooling input fell below 0.3 °C and development density was high, creating persistent urban heat hotspots. Cooling benefits remained concentrated in the park core while thermal stress extended outward.

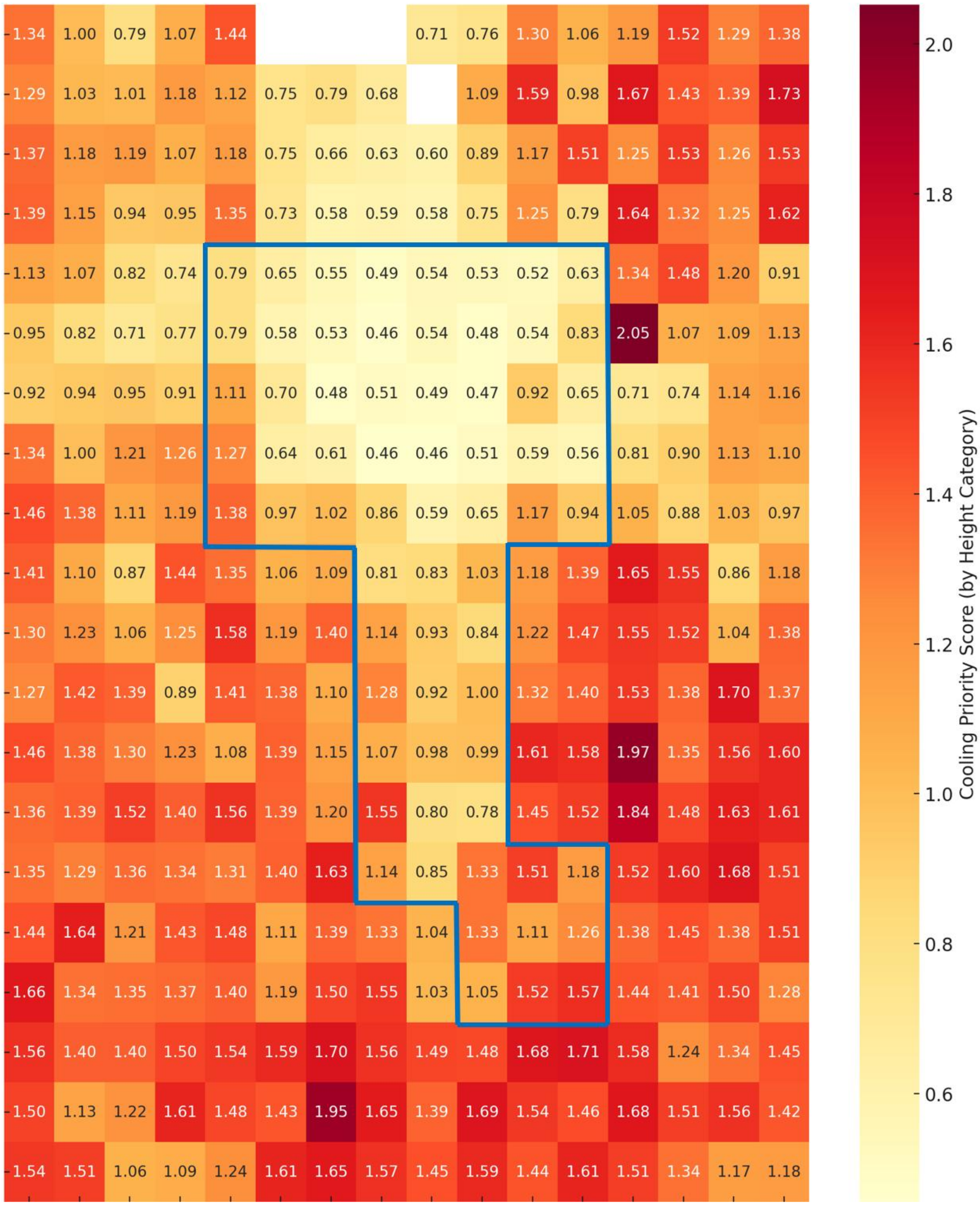

Figure 8. Spatial distribution pattern of adjustment gap priority score.

4. Discussion

4.1. Supply Variation in Cooling Service Across Land Cover Types

Monitoring results across spatial and temporal scales consistently showed that tree-covered areas offer the most stable and effective cooling compared with water, grass, and impervious surfaces because of their combined shading and evapotranspiration effects, highlighting their crucial role in mitigating urban heat. Numerous studies highlighted that larger green patches with high tree density consistently showed stronger regulation primarily through extensive shading and evaporative cooling that replaced sensible heat with latent heat (Moss et al., 2019; Rendon et al., 2024; Richards et al., 2020) . This supported our observed hierarchy of trees first, followed by water and grass. Rahman et al. (2024) emphasized that transpiration alone cannot offset strong solar heating without tree shade. Trees change temperature and relative humidity in two ways, one is reducing the underlying surface temperature by shading(Armson et al., 2012; Horvathova et al., 2021). Most of the tree species in Beijing Olympic Park were mixed coniferous and broadleaved forests, with high height and long planting time, which enhanced their ability to control land surface temperature changes in the surrounding areas (Kowalska et al., 2025; Kuang et al., 2020). The other way is directly affecting the air flow through the leaves by photosynthesis, and water in the leaves evaporates. The evaporative cooling rate is related to air humidity difference and air flow rate. When the wind speed is low, the cooling effect is strongest, but the affected air volume is small. Higher wind speeds bring in fresher air, extending the impact range but reducing the intensity of monomer cooling (Oke et al., 2017). The strong wind speed in Beijing expanded the radiation range of cooling service flow of tree land. Our results also showed that the continuous and large water body of the Olympic Park's cooling effect is strong. Previous studies on 36 parks in Zhengzhou identified water areas as a key cooling factor, but water's effect depends on context (Gao et al., 2023). Large or flowing water under dry, windy conditions may cool effectively while small, stagnant ponds on humid days may offer limited benefit (Hu et al., 2019). This contrast suggests that local climate and park design, such as water size, depth and nearby vegetation, influence water's cooling role.

4.2. Spatial Diffusion of Cooling Flows and Factors Constraining The Reach

Our findings aligned with empirical studies showing that park cooling effects generally tapered off within several city blocks to about 1 km. Qiu & Jia (2020) noted that in many cities cooling was concentrated within 600 to 1000 m of large parks, beyond which it faded into the ambient urban heat island conditions. In our case the Beijing Olympic Park which covers more than 6.8 km² and is densely vegetated, extended this range to nearly 2 km. Comparable distances had been reported for expansive green spaces in Mexico City under favorable conditions (Oke et al., 2017). Even for parks of this scale however the marginal effect beyond 1 km declined sharply. In our data temperature reductions beyond the 1 km buffer dropped below 0.5 °C and effectively blended into the surrounding urban thermal environment. These observations reinforced that a single park's cooling was spatially limited and insufficient for distant urban areas (Silveira et al., 2024; Verma et al., 2024). The extent of park cooling depended on park size and vegetation density as well as urban morphology and atmospheric conditions (Zaki et al., 2020). The dense part of green space in the north of Beijing Olympic Park has a better service radiation effect, while the south part is dominated by buildings and is closer to city center, thus its weak radiation ability is integrated into the urban thermal environment background (Sun et al., 2025). A potential mechanistic explanation for this imbalance is that high-density built environments near the city center generate more heat and obstruct the movement of cool air so that localized hotspots occur even near large green spaces (Chen et al., 2020; Yang et al., 2025).

To mitigate these effects urban planners should enhance landscape permeability around parks. Recommended strategies include protecting and expanding green corridors maintaining wind corridors or controling building heights in key sectors and adding small green patches as stepping stones to extend cooling influence. Such measures are consistent with climate sensitive urban design concepts ventilation corridors and greenway networks. He et al. (2024) recommended linking open spaces to guide park breezes through the city and Norton et al. (2015) advocated integrating green infrastructure at the city scale. Although the natural decay of park cooling cannot be avoided, its steepness may be moderated by thoughtful urban planning that promotes cold air diffusion and prevents thermal enclaves immediately beyond major green spaces (Kim et al., 2024; T. Zhang et al., 2024).

4.3. Supply-Demand Mismatches and Identification of Thermal Regulation Gaps

In our analysis, we quantitatively identified cooling gaps within one to two kilometers surrounding the Beijing Olympic Park, with the most pronounced mismatches occurring in the southwestern and northeastern sectors. In these areas, unmet cooling demand reached approximately 7.5 °C, while modeled cooling supply remained below 0.3 °C. By weighting demand based on building typologies categorized by height, we found that even spatially proximate areas could exhibit markedly different levels of supply–demand mismatch. The highest-priority zones were primarily composed of densely built commercial areas such as the central business district, where high-rise structures and sparse vegetation dominate (Li and Sun, 2023b). This pattern is consistent with previous findings (Liyan et al., 2023), and may be explained that rapid urban development and high construction intensity tend to reduce the cooling efficiency of green spaces Guan & Zhang (2024). In densely populated areas, this often offsets the cooling benefits provided by urban parks. Such mismatches in ecosystem service supply and demand are not unique to Beijing. For example, Baró et al. (2016) reported that in Barcelona, highly built-up neighborhoods were exposed to elevated thermal stress, while the cooling benefits of urban green infrastructure were limited, resulting in heat-vulnerable zones. And a broader study across multiple European cities further indicated that in most identified mismatches, regulating ecosystem services provided by green infrastructure played only a secondary or complementary role in mitigating urban-scale air pollution and greenhouse gas emissions (Baró et al., 2015). Implementing urban forestry and shade-providing infrastructure around hotspot zones near parks could significantly enhance Beijing's thermal resilience. Bridging these service gaps may also yield feedback benefits, allowing the cooling function of parks to become more effective over time.

4.4. Methodological Contributions and Transferability of the Supply-Flow-Demand Framework

Beyond site-specific findings, this study offers a methodological framework for assessing urban park's cooling services within an integrated supply–flow–demand perspective. Departing from traditional land-based evaluations, we adopt a human-centered perspective that explicitly links cooling supply to beneficiary needs. Zhou et al. (2024) emphasized that urban park planning should account for demographic distributions to enhance the relevance of ecosystem services. Using the InVEST Urban Cooling model, we quantified service supply through a unified thermal mitigation index and coupled it with building-level cooling demand derived from outdoor comfort exceedance and height-based energy sensitivity.

A key strength of our approach lies in its ability to spatially identify mismatches between ecosystem service supply and demand, thereby directly supporting climate-responsive urban planning. The framework is adaptable and replicable across cities, relying on accessible inputs such as land cover, surface temperature, and comfort thresholds, alongside open-source InVEST tools. Moreover, by incorporating energy coefficients specific to building height, we bridge the gap between ecological metrics and tangible outcomes related to energy use and human thermal comfort, enhancing the policy relevance of our results (Haase and Dushkova, 2024; Wolff et al., 2015).

We acknowledge several limitations and future applications of this model. First, our analysis focused on daytime summer conditions and did not consider nighttime or winter dynamics, which may alter cooling patterns. Second, our demand metric did not account for indoor exposure, vulnerable populations, or adaptive behaviors. Future iterations could be improved by integrating data on energy use or heat-related health risks. Additionally, the model assumes static land cover and meteorological conditions, while real urban environments experience shifting winds, humidity, and development pressures. Despite these limitations, our approach provides a valuable reference for quantifying the spatial flow of park-based cooling services within a unified grid framework. As cities face intensifying urban heat, such integrated assessments can inform more strategic and equitable investments in green infrastructure, ensuring that cooling services are delivered where they are most needed and have the greatest impact.

5. Conclusions

In this study we have established a spatially explicit supply–flow–demand framework to quantify the cooling services of a large urban park and to reveal where those services fall short of surrounding thermal needs. By integrating field-based heat index measurements with the InVEST Urban Cooling Model we demonstrated that tree-dominated areas within Beijing Olympic Park deliver the most stable and intense cooling. Coupling modeled cooling supply with building-level demand exposed clear spatial mismatches. Areas 1-2 km from the park edge, characterized by dense built environments and scarce vegetation, experienced unmet cooling needs of up to 7.5℃. The introduction of a gap index and a priority score has pinpointed these hotspots and provided a quantitative basis for targeting interventions in the most vulnerable neighbourhoods. Our methodological contributions lie in linking ecosystem service modeling to human comfort and energy sensitivity through a uniform grid system and in offering a transferable approach for other cities. As cities confront intensifying heat stress, targeted and equitable investment in green infrastructure informed by supply-flow-demand analysis will be essential to ensure that cooling services are delivered where they are needed most.

Declaration of generative AI and AI-assisted technologies in the writing process

During the preparation of this work the authors used ChatGPT to improve language clarity and consistency. After using this tool, the authors reviewed and edited the content and take full responsibility for the content of the publication.

Reference:

Aflaki, A., Mirnezhad, M., Ghaffarianhoseini Amirhosein and Ghaffarianhoseini, A., Omrany, H., Wang, Z.-H., Akbari, H., 2017. Urban heat island mitigation strategies: A state-of-the-art review on Kuala

Lumpur, Singapore and Hong Kong. CITIES 62, 131–145. https://doi.org/10.1016/j.cities.2016.09.003

Alves, F.M., Goncalves, A., del Caz-Enjuto, M.R., 2022. The Use of Envi-Met for the Assessment of Nature-Based Solutions' Potential Benefits in Industrial Parks-A Case Study of Argales Industrial Park (Valladolid, Spain). Infrastructures (Basel) 7. https://doi.org/10.3390/infrastructures7060085

Amani-Beni, M., Zhang, B., Xie, G., Xu, J., 2018. Impact of urban park's tree, grass and waterbody on microclimate in hot summer days: A case study of Olympic Park in Beijing, China. Urban For Urban Green 32, 1–6. https://doi.org/10.1016/j.ufug.2018.03.016

Aram, F., Higueras Garcia, E., Solgi, E., Mansournia, S., 2019. Urban green space cooling effect in cities. Heliyon 5. https://doi.org/10.1016/j.heliyon.2019.e01339

Armson, D., Stringer, P., Ennos, A.R., 2012. The effect of tree shade and grass on surface and globe temperatures in an urban area. Urban For Urban Green 11, 245–255. https://doi.org/10.1016/j.ufug.2012.05.002

Baró, F., Haase, D., Gómez-Baggethun, E., Frantzeskaki, N., 2015. Mismatches between ecosystem services supply and demand in urban areas: A quantitative assessment in five European cities. Ecol Indic 55, 146–158. https://doi.org/10.1016/j.ecolind.2015.03.013

Baró, F., Palomo, I., Zulian, G., Vizcaino, P., Haase, D., Gómez-Baggethun, E., 2016. Mapping ecosystem service capacity, flow and demand for landscape and urban planning: A case study in the Barcelona metropolitan region. Land use policy 57, 405–417. https://doi.org/10.1016/j.landusepol.2016.06.006

Buccolieri, R., Santiago, J.-L., Rivas, E., Sanchez, B., 2018. Review on urban tree modelling in CFD simulations: Aerodynamic, deposition and thermal effects. Urban For Urban Green 31, 212–220. https://doi.org/10.1016/j.ufug.2018.03.003

Chen, Y., Wu, J., Yu, K., Wang, D., 2020. Evaluating the impact of the building density and height on the block surface temperature. Build Environ 168. https://doi.org/10.1016/j.buildenv.2019.106493

Droogers, P., Allen, R.G., 2002. Estimating Reference Evapotranspiration Under Inaccurate Data Conditions. Irrigation and Drainage Systems 16, 33–45. https://doi.org/10.1023/A:1015508322413

Ebi, K.L., Capon, A., Berry, P., Broderick, C., de Dear, R., Havenith, G., Honda, Y., Kovats, R.S., Ma, W., Malik, A., Morris, N.B., Nybo, L., Seneviratne, S.I., Vanos, J., Jay, O., 2021. Hot weather and heat extremes: health risks. LANCET 398, 698–708.

Fang, X., Li, J., Ma, Q., Zhou, R., Du, S., 2024. A quantitative review of nature-based solutions for urban sustainability (2016-2022): From science to implementation. SCIENCE OF THE TOTAL ENVIRONMENT 927. https://doi.org/10.1016/j.scitotenv.2024.172219

Fang, Y., Zhao, L., 2024. Exploring the supply-demand match and drivers of blue-green spaces cooling in Wuhan Metropolis. Urban Clim 58. https://doi.org/10.1016/j.uclim.2024.102194

Gao, Y., Pan, H., Tian, L., 2023. Analysis of the spillover characteristics of cooling effect in an urban park: A case study in Zhengzhou city. Front Earth Sci (Lausanne) 11. https://doi.org/10.3389/feart.2023.1133901

Guan, Z., Zhang, H., 2024. A Quantitative Analysis of the Complex Response Relationship between Urban Green Infrastructure (UGI) Structure/Spatial Pattern and Urban Thermal Environment in Shanghai. Sustainability 16. https://doi.org/10.3390/su16166886

Haase, D., Dushkova, D., 2024. Embracing ambivalence as the key to promoting tree diversities as nature-based solutions in European cities. Urban Ecosyst 27, 1837–1846. https://doi.org/10.1007/s11252-024-01555-9

He, Y., Wong, C.H.M., Deng, J., Liu, Z., Ng, E., 2024. Designing breezeways to enhance wind environments in high-density cities: A comprehensive analysis of ten morphological parameters. Sustain Cities Soc 116. https://doi.org/10.1016/j.scs.2024.105898

Horvathova, E., Badura, T., Duchkova, H., 2021. The value of the shading function of urban trees: A replacement cost approach. Urban For Urban Green 62. https://doi.org/10.1016/j.ufug.2021.127166

Hu, L., Wilhelmi, O. V, Uejio, C., 2019. Assessment of heat exposure in cities: Combining the dynamics of temperature and population. SCIENCE OF THE TOTAL ENVIRONMENT 655, 1–12. https://doi.org/10.1016/j.scitotenv.2018.11.028

Jay, O., Capon, A., Berry, P., Broderick Carolyn and de Dear, R., Havenith, G., Honda, Y., Kovats, R.S., Ma, W., Malik, A., Morris, N.B., Nybo, L., Seneviratne, S.I., Vanos, J., Ebi, K.L., 2021. Reducing the health effects of hot weather and heat extremes: from personal cooling strategies to green cities. LANCET 398, 709–724.

Kim, J.Y., Park, C.Y., Lee, D.K., Yun, S.H., Hyun, J.H., Kim, E.S., 2024. The cooling effect of trees in high-rise building complexes in relation to spatial distance from buildings. Sustain Cities Soc 114. https://doi.org/10.1016/j.scs.2024.105737

Kowalska, A., Affek, A.N., Wolski, J., Regulska, E., 2025. Ranking Warsaw green spaces by cooling efficiency and particulate matter deposition potential for spatial planning. Sustain Cities Soc 118. https://doi.org/10.1016/j.scs.2024.106064

Kuang, W., Li, Z., Hamdi, R., 2020. Comparison of surface radiation and turbulent heat fluxes in Olympic Forest Park and on a building roof in Beijing, China. Urban Clim 31. https://doi.org/10.1016/j.uclim.2019.100562

Lai, Z., He, J., Li, Y., 2024. Potential zones identification for district cooling system: A GIS-based multi-criteria assessment method incorporating cooling demand mapping. Sustain Cities Soc 105, 105327. https://doi.org/https://doi.org/10.1016/j.scs.2024.105327

Lan, H., Zhang, Y., Yang, Y., Zhao, X., Yu, T., Li, X., Wang, B., Xie, Y., 2025. Analyzing inequities in vegetation cooling services along the urban-rural gradient using the LAI-integrated InVEST urban cooling model. Urban For Urban Green 104, 128665. https://doi.org/10.1016/j.ufug.2024.128665

Li, W., Sun, R., 2023a. A supply-demand model of vegetation cooling for urban heatwave mitigation. Urban Clim 52, 101699. https://doi.org/10.1016/j.uclim.2023.101699

Li, W., Sun, R., 2023b. A supply-demand model of vegetation cooling for urban heatwave mitigation. Urban Clim 52, 101699. https://doi.org/10.1016/j.uclim.2023.101699

Li, Y., Fan, S., Li, K., Zhang, Y., Kong, L., Xie, Y., Dong, L., 2021. Large urban parks summertime cool and wet island intensity and its influencing factors in Beijing, China. Urban For Urban Green 65. https://doi.org/10.1016/j.ufug.2021.127375

Lin, Y., Chen, X., Huang, L., Zhu, C., Shahtahmassebi, A., Zhang, J., Shen, S., Peng, R., Deng, J., Wang, K., Gan, M., 2021. Fine-scale mapping of urban ecosystem service demand in a metropolitan context: A population-income-environmental perspective. SCIENCE OF THE TOTAL ENVIRONMENT 781. https://doi.org/10.1016/j.scitotenv.2021.146784

Liyan, X., Yin, H., Fang, J., 2023. Evaluating the supply-demand relationship for urban green parks in

Beijing from an ecosystem service flow perspective. Urban For Urban Green 85, 127974. https://doi.org/10.1016/j.ufug.2023.127974

Markevych, I., Schoierer, J., Hartig, T., Chudnovsky, A., Hystad, P., Dzhambov, A.M., de Vries Sjerp and Triguero-Mas, M., Brauer, M., Nieuwenhuijsen, M.J., Lupp, G., Richardson, E.A., Astell-Burt Thomas and Dimitrova, D., Feng, X., Sadeh, M., Standl Marie and Heinrich, J., Fuertes, E., 2017. Exploring pathways linking greenspace to health: Theoretical and methodological guidance. Environ Res 158, 301–317. https://doi.org/10.1016/j.envres.2017.06.028

Mashhoodi, B., 2021. Environmental justice and surface temperature: Income, ethnic, gender, and age inequalities. Sustain Cities Soc 68. https://doi.org/10.1016/j.scs.2021.102810

Mi, Z., Guan, D., Liu, Z., Liu, J., Viguie, V., Fromer, N., Wang, Y., 2019. Cities: The core of climate change mitigation. J Clean Prod 207, 582–589. https://doi.org/10.1016/j.jclepro.2018.10.034

Moss, J.L., Doick, K.J., Smith, S., Shahrestani, M., 2019. Influence of evaporative cooling by urban forests on cooling demand in cities. Urban For Urban Green 37, 65–73. https://doi.org/10.1016/j.ufug.2018.07.023

Mosteiro-Romero, M., Maiullari, D., Pijpers-van Esch, M., Schlueter, A., 2020. An Integrated Microclimate-Energy Demand Simulation Method for the Assessment of Urban Districts. Front Built Environ 6. https://doi.org/10.3389/fbuil.2020.553946

Norton, B.A., Coutts, A.M., Livesley, S.J., Harris, R.J., Hunter, A.M., Williams, N.S.G., 2015. Planning for cooler cities: A framework to prioritise green infrastructure to mitigate high temperatures in urban landscapes. Landsc Urban Plan 134, 127–138. https://doi.org/10.1016/j.landurbplan.2014.10.018

Oke, T., Mills, G., Christen, A., Voogt, J., 2017. Urban Climates, Urban Climates. https://doi.org/10.1017/9781139016476

Qiu, K., Jia, B., 2020. The roles of landscape both inside the park and the surroundings in park cooling effect. Sustain Cities Soc 52. https://doi.org/10.1016/j.scs.2019.101864

Rahman, T., Suhendri, Tajudin, A.N., Suwarto, F., Sudigdo, P., Thom, N., 2024. Durability evaluation of heat-reflective coatings for road surfaces: A systematic review. Sustain Cities Soc 112. https://doi.org/10.1016/j.scs.2024.105625

Rendon, P., Love, N., Pawlak, C., Yost, J., Ritter, M., Doremus, J., 2024. Street tree diversity and urban heat. Urban For Urban Green 91. https://doi.org/10.1016/j.ufug.2023.128180

Richards, D.R., Fung, T.K., Belcher, R.N., Edwards, P.J., 2020. Differential air temperature cooling performance of urban vegetation types in the tropics. Urban For Urban Green 50. https://doi.org/10.1016/j.ufug.2020.126651

Silveira, C., Amaral, F.G., Dias, A.T.C., de Gois, G., Piston, N., 2024. The importance of private gardens and their spatial composition and configuration to urban heat island mitigation. Sustain Cities Soc 112. https://doi.org/10.1016/j.scs.2024.105589

Sun, X., Fang, P., Huang, S., Liang, Y., Zhang, J., Wang, J., 2025. Impact of urban green space morphology and vegetation composition on seasonal land surface temperature: a case study of Beijing's urban core. Urban Clim 60. https://doi.org/10.1016/j.uclim.2025.102367

Toparlar, Y., Blocken, B., Maiheu, B., van Heijst, G.J.F., 2017. A review on the CFD analysis of urban microclimate. RENEWABLE & SUSTAINABLE ENERGY REVIEWS 80, 1613–1640. https://doi.org/10.1016/j.rser.2017.05.248

Verma, R., Zawadzka, J.E., Garg, P.K., Corstanje, R., 2024. The relationship between spatial configuration of urban parks and neighbourhood cooling in a humid subtropical city. Landsc Ecol 39. https://doi.org/10.1007/s10980-024-01818-y

Wang, R., Lu, T., He, B., Wang, F., Huang, Q., Qian, Z., Min, J., Li, Y., 2024. Seasonal urban surface thermal environment analysis based on local climate zones: A case study of Chongqing. SCIENCE OF THE TOTAL ENVIRONMENT 954. https://doi.org/10.1016/j.scitotenv.2024.176577

Wang, W., He, J., Wang, X., 2024. Quantitatively comparing the morphological influences on the cool island effect in urban waterfront blue-green spaces across six cities near 30°N. Urban Clim 56. https://doi.org/10.1016/j.uclim.2024.102076

Wang, Y., Ouyang, W., Zhang, J., 2024. Matching supply and demand of cooling service provided by urban green and blue space. Urban For Urban Green 96, 128338. https://doi.org/10.1016/j.ufug.2024.128338

Wolff, S., Schulp, C.J.E., Verburg, P., 2015. Mapping ecosystem services demand: A review of current research and future perspectives. Ecol Indic 55. https://doi.org/10.1016/j.ecolind.2015.03.016

Xiao, Y., Piao, Y., Wei, W., Pan, C., Lee, D., Zhao, B., 2023. A comprehensive framework of cooling effect-accessibility-urban development to assessing and planning park cooling services. Sustain Cities Soc 98. https://doi.org/10.1016/j.scs.2023.104817

Xiong, Y., Peng, F., Zou, B., 2019. Spatiotemporal influences of land use/cover changes on the heat island effect in rapid urbanization area. Front Earth Sci 13, 614–627. https://doi.org/10.1007/s11707-018-0747-3

Yang, M., Nie, W., Wu, R., Yan, H., Tian, S., Wang, K., Shi, L., Cheng, X., Ji, T., Bao, Z., 2024. Towards more equitable cooling services of urban parks: Linking cooling effect, accessibility and attractiveness. J Environ Manage 370. https://doi.org/10.1016/j.jenvman.2024.122475

Yang, S., Wang, L. (Leon), Stathopoulos, T., Marey, A.M., 2023. Urban microclimate and its impact on built environment-A review. Build Environ 283. https://doi.org/10.1016/j.buildenv.2023.110334

Yang, Y., Lv, Y., Zhou, D., 2025. The impact of urban parks on the thermal environment of built-up areas and an optimization method. PLoS One 20. https://doi.org/10.1371/journal.pone.0318633

Zaki, S.A., Othman, N.E., Syahidah, S.W., Yakub, F., Muhammad-Sukki, F., Ardila-Rey, J.A., Shahidan, M.F., Saudi, A.S.M., 2020. Effects of Urban Morphology on Microclimate Parameters in an Urban University Campus. Sustainability 12. https://doi.org/10.3390/su12072962

Zeng, P., Liu, Y., Tian, T., Che, Y., Helbich, M., 2024. Geographic inequalities in park visits to mitigate thermal discomfort: A novel approach based on thermal differences and cellular population data. Urban For Urban Green 98. https://doi.org/10.1016/j.ufug.2024.128419

Zhang, N., Zhen, W., Shi, D., Zhong, C., Li, Y., 2024. Quantification and mapping of the cooling effect of urban parks on the temperate monsoon climate zone. Sustain Cities Soc 101. https://doi.org/10.1016/j.scs.2023.105111

Zhang, T., Fu, X., Qi, F., Shen, Y., 2024. Study on the daily thermal radiation iso-disturbance on a building by trees in summer. Urban For Urban Green 99. https://doi.org/10.1016/j.ufug.2024.128468

Zhou, W., Wu, T., Tao, X., 2024. Exploring the spatial and seasonal heterogeneity of cooling effect of an urban river on a landscape scale. Sci Rep 14. https://doi.org/10.1038/s41598-024-58879-x